# MECHANISMS OF COMPRESSIVE FAILURE IN WOVEN COMPOSITES AND STITCHED LAMINATES



B.N. Cox, M.S. Dadkhah, R.V. Inman, W.L. Morris, and S. Schroeder
Rockwell International Science Center
1049 Camino Dos Rios
Thousand Oaks, CA

## ABSTRACT

Stitched laminates and angle interlock woven composites have been studied in uniaxial, in-plane, monotonic compression. Failure mechanisms have been found to depend strongly on both the reinforcement architecture and the degree of constraint imposed by the loading grips. Stitched laminates show higher compressive strength, but are brittle, possessing no load bearing capacity beyond the strain for peak load. Post-mortem inspection shows a localized shear band of buckled and broken fibers, which is evidently the product of an unstably propagating kink band. Similar shear bands are found in the woven composites if the constraint of lateral displacements is weak; but, under strong constraint, damage is not localized but distributed throughout the gauge section. While the woven composites tested are weaker than the stitched laminates, they continue to bear significant loads to compressive strains of ~ 15%, even when most damage is confined to a shear band.

## 1. INTRODUCTION

One of the principal weaknesses of conventional, two-dimensional (2D) polymer composites is their vulnerability to delamination, particularly under compressive loading following impact. This problem has led to the accelerated development of polymer composites reinforced by various three-dimensional (3D) arrangements of fibers, with the general goal of enhancing through-thickness strength without degrading in-plane strength or stiffness (refs. 1-4). All forms of 3D architectures are under study in this quest, including structures manufactured by weaving, stitching, knitting, and braiding; and there has been considerable success in eliminating the delamination problem. Unfortunately, this particular improvement has generally come at the expense of other material properties, such as fatigue resistance and strength.

While there is thus much room for improving 3D composites, there is not yet any understanding of how to set about this systematically. The challenge of choosing from the infinite variety of available reinforcement architectures is compounded by ignorance of how particular geometrical features in the arrangement of fibers might influence failure mechanisms.

This paper begins to address these questions by a comparison of stitched laminates and certain woven composites under monotonic compression. Striking differences are found in the strength and strains to failure for the two classes of material, stitched laminates exhibiting brittle behavior and woven composites ductile behavior. These observations are related to differences in the fiber architecture, suggesting some fundamental concepts for 3D composite behavior, which may guide the way to optimizing strength and damage tolerance and in mapping out failure modes.

## 2. SPECIMENS

### 2.1 Stitched Laminates

Stitched laminates were manufactured by Douglas Aircraft Co.‡ They consist of 48 plies of AS4 carbon fibers in the quasi-isotropic lay-up $(+45°/0°/-45°/90°)_{6S}$, stitched with carbon, glass, or Kevlar fibers. In fact, each ply is in itself a 2D woven fabric ("uniweave") in which the AS4 fibers have been woven in a plain weave with a small quantity of glass fibers to facilitate handling during stacking and stitching. The AS4 fiber tows serve as warp yarns in this weaving step and constitute 95 percent of the fabric by weight, while the glass fibers are incorporated as fill (weft yarns) and constitute the remainder. Some kinking of the AS4 fibers is inevitable during weaving, but it appears that neither the kinking nor the presence of the woven glass fibers has a strong influence on failure mechanisms (see below). In describing the stacking sequence of the laminate, the angle of each ply refers to the angle of the AS4 fibers.

Following stacking, the lay-up was stitched in rows along both the 0° and 90° directions, using modified lock stitching (Fig. 1). The bobbin threads, which are primarily responsible for 3D reinforcement, consist of one of three kinds of yarn, as listed in Table 1. While in all cases there are nominally 1.6 rows of stitches per cm. (4 per inch) in both the 0° and 90° directions, the number of stitches per cm. within each row varies with stitching direction and from specimen to specimen. Average, measured values are given in Table 1. Table 1 also shows the volume fractions of the stitching fibers (referring only to those segments of stitching tows lying in the through-thickness directions) estimated from these data and specific gravities. The final entry of Table 1 shows the volume fraction of 0° AS4 fibers estimated from micrographs of cross sections.

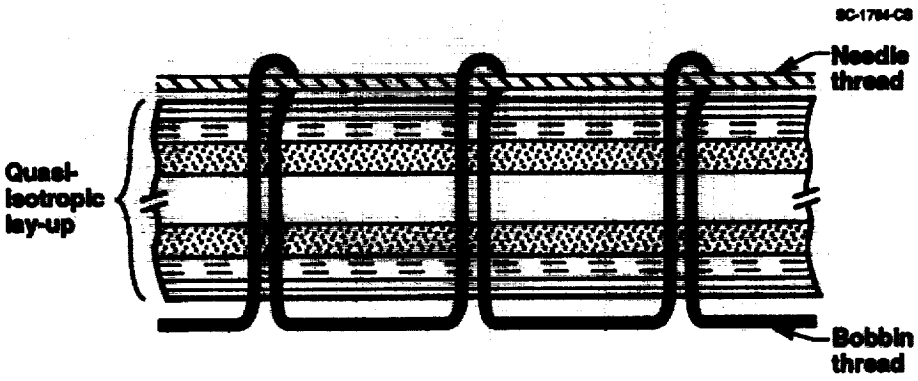


Fig. 1 Schematic of quasi-isotropic laminate reinforced by modified lock stitching.

The stitched preforms were impregnated with 3501-6 resin by resin transfer moulding and the resin was cured (ref. 5).

### 2.2 Woven Composites

All woven fiber preforms were supplied by Textile Technologies Inc.* They were either through-the-thickness or layer-to-layer angle interlock weaves, as illustrated in Fig. 2. All

‡Douglas Aircraft Co., Long Beach, California.
*Textile Technologies, Inc., Hatboro, Pennsylvania.

stuffer (or straight warp) and filler (or weft) fiber tows were 2lk denier* AS4 carbon yarns. Warp weaver (or 3D warp) fiber tows were either 9k denier AS4 carbon yarns or 5.95k denier S-2 glass yarns. The stuffers and fillers form a relatively coarse 0°/90° laminate, while the warp weaver tows follow approximately sawtooth paths, binding fillers and therefore stuffers together in the through-thickness direction. Figure 2 shows projections of the weave pattern along the weft direction.

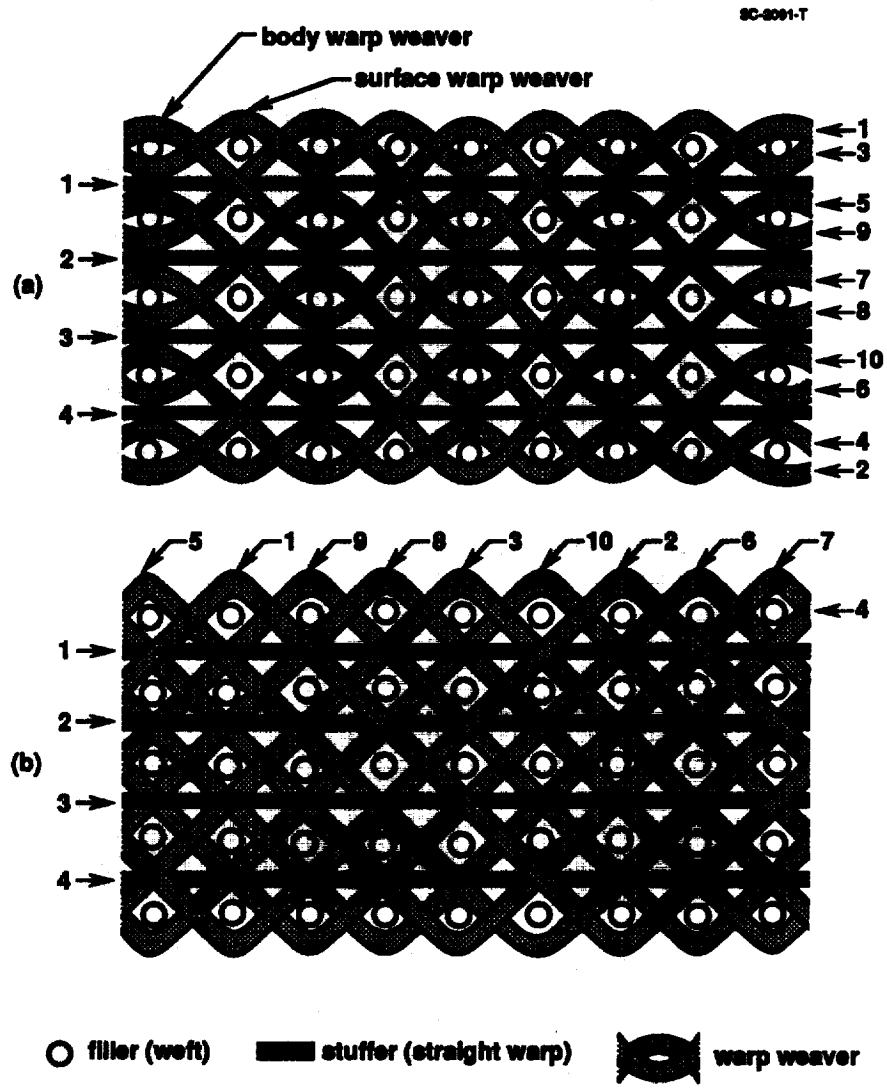


Fig. 2 Schematic of the projection of (a) layer-to-layer and (b) through-the-thickness angle interlock fiber preforms onto a plane normal to the weft tows.

The weaver's nominal specifications of the number of columns of fillers per cm. in the warp direction and the number of columns of stuffers (and therefore pairs or quartets of warp weavers) per cm. in the weft direction are given in Table 2, along with measured thicknesses of the dry preforms. Noting that the density of AS4 carbon is 1.8 g/cm$^3$ and that of S-2 glass 2.48 g/cm$^3$ (e.g. (ref. 6)), and approximating the length of each warp weaver per cm. in the warp direction as $\sqrt{2}$ cm., one can estimate the nominal volume fractions of the various fibers from these data. These results are also shown in Table 2. In the case of the layer-to-layer

*Denier measures the weight in grams of 9000 meters of yarn.

architecture, the volume fraction of warp weavers includes only the body warp weavers of Fig. 2(a).

In practice, considerable deviance from the nominal volume fractions is found in actual specimens, as detailed below. Furthermore, the surface warp weavers in specimens of type A were found not to be curved, as in the specification of Fig. 2(a), but straight. In assessing effects of the volume fraction of fibers aligned along the load axis, they were therefore added to the stuffers in estimating $v_s$, giving values on average 20% higher than those of Table 2 (see below).

Impregnation and cure of the woven preforms were carried out by the authors, using methods developed *ad hoc*. The matrix in all cases was formed from Tactix 138 resin and H41 hardener (Dow Chemical‡). The preform was placed in a reusable aluminum mould, heated to 65°C, and degassed in a vacuum of ~ 1 Torr. The resin was then mixed with the hardener and also heated to 65°C and degassed. The resin and hardener were then poured over the preform (still at 65°C and under vacuum) and the whole assembly was degassed twice again. The first degassing typically resulted in bubbling out of some volatiles followed by apparent boiling of the resin-hardener mixture as the pressure fell further. The pressure was then cycled between 1 Torr and atmospheric pressure to remove small bubbles clinging to the mat. The mould was then closed and the specimen cured, the curing cycle (chosen to maximize resin toughness) comprising 2 hrs at 120°C and 2 hrs at 177°C. All fabrication runs produced 25 cm × 10 cm panels, from which specimens were machined.

There was no visible porosity in any specimen. Furthermore, the only microcracks to be found were confined to surface pockets of resin between tows. Detailed observations of failure mechanisms revealed that these initial surface microcracks have no role in compressive failure.

During impregnation and cure, a small pressure was applied through the thickness of the preform by screwing down the lid of the mould. This pressure was sufficient to ensure firm contact between the mould and the thicker parts of the preform, but not sufficient to maximize fiber packing density elsewhere. It was felt that attempting to do so would have led to fiber kinking where the preform was thickest, which would be likely to degrade compressive strength. If more uniform preforms become available in the future, significant enhancement of the fiber volume fractions should be feasible. It is likely that compressive strength would then also rise.

## 3. UNIAXIAL COMPRESSION TESTS

The first tests to be described were conducted on cuboidal specimens approximately 2.1 cm long and 1 cm wide, with the thickness being that of the panel. The length of each composite specimen was aligned with the warp direction for woven composites and the 0° ply direction for stitched laminates. The length also coincided with the load axis. Uniaxial compression tests for these specimens were conducted under displacement control in a 20 kip MTS test machine, with the ends of the specimen loaded by flat platens. There was no evidence of slip between the platens and the specimen ends, so that the stress state in the specimens was nonuniform, with deformation near the specimen ends being highly constrained. Results are summarized in Table 3. The epoxy specimens of Table 3 consisted of neat resin cured according to the cycle defined in the preceding section.

Some further tests were conducted for the woven composites using dog-bone specimens with gauge sections 2.4 cm long and 1.1 cm wide. Once again, the load axis and length of the

‡Dow Chemical, Freeport, Texas.

dog-bone specimens coincided with the stuffers, while the direction normal to the flat faces of the specimens was that of the through-thickness reinforcement. Loading was effected by a 200 kip hydraulic machine with aligning hydraulic grips.

### 3.1 Strength and Strain to Failure

Cuboidal Specimen Test Results

Stress-strain curves for cuboidal specimens of stitched laminates and woven composites are shown in Fig. 3. The effective initial composite modulus, the maximum compressive load sustained, the strain $\varepsilon_m$ at which it occurs, and the strain, $\varepsilon_{1/2}$, at which the load had fallen to 50% of its maximum after peak load, are also presented numerically in Table 3.

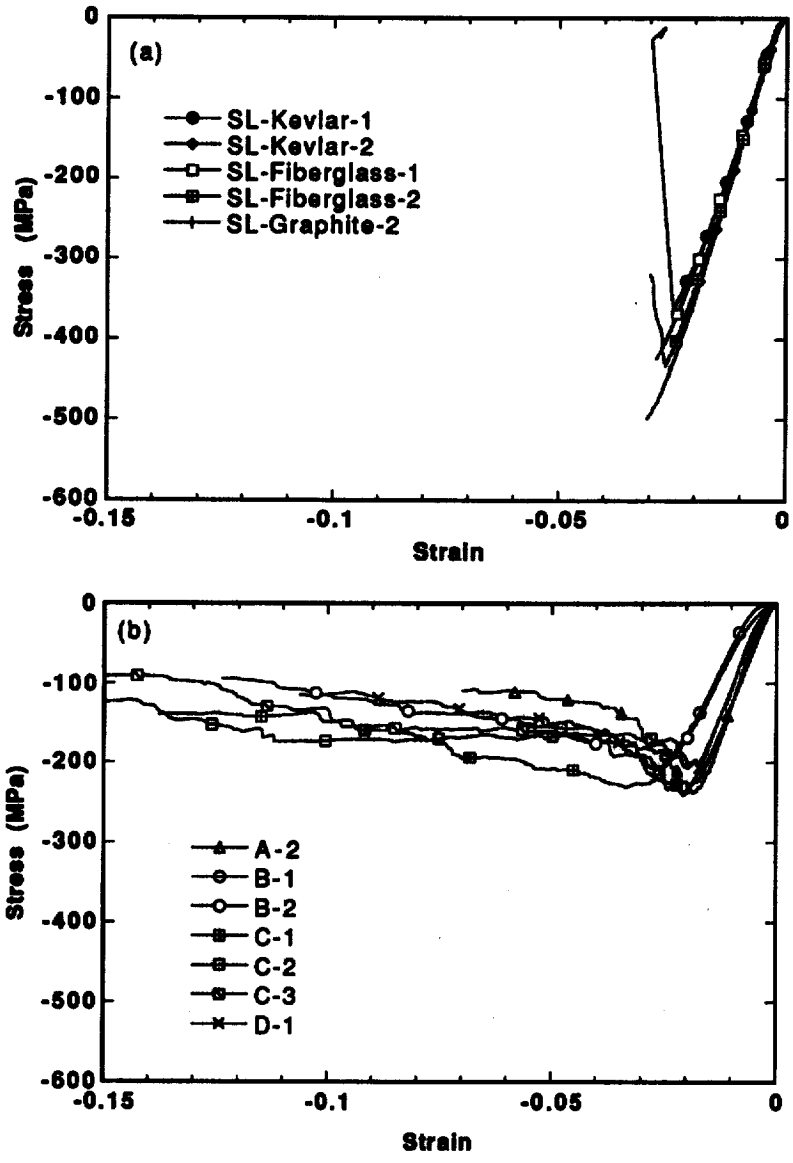


Fig. 3 Strain-load histories for cuboidal specimens under uniaxial compression. (a) Stitched laminates. (b) Woven composites. Legends refer to the nomenclature of Table 3.

For stitched laminates (Fig. 3(a)), the response is initially linear, the apparent non-linearity at very small loads merely reflecting slack space being taken up between the specimens and the platens. (All strains in Table 3 were adjusted to compensate for this effect by exatrapolating back from the linear regime to redefine the origin.) There is a moderate decrease in modulus somewhat before failure, which occurs at compressive stresses between 360 and 495 MPa. There is essentially no load bearing capacity at higher strains, indicating that failure is catastrophic. Post-mortem examination reveals the damage typified by Fig. 4(a): damage is confined to a narrow shear band traversing the thickness of the specimen. Within this band, plies are buckled and failed and nearly all plies are delaminated from one another. The damage extends in the 0° ply direction over a distance comparable to the stitching spacing, but the stitches have played no obvious part in initiating or moderating failure.

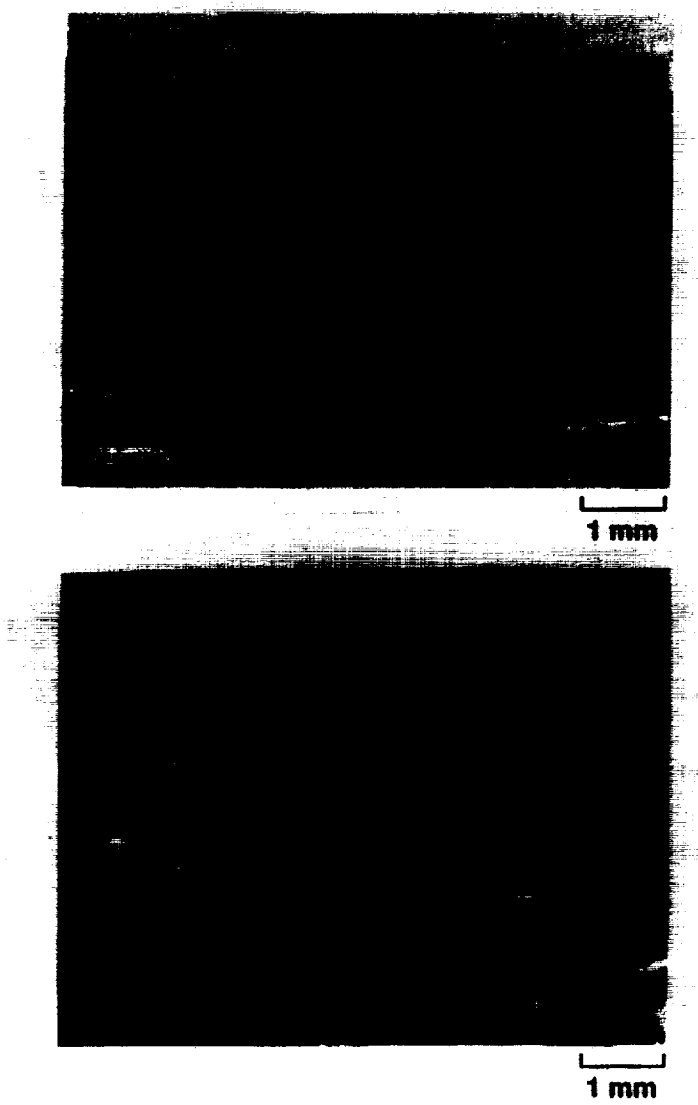


Fig. 4 Damage in cuboidal specimens of (a) a stitched laminate (SL-Kevlar-1 of Table 3) and (b) a woven composite (through-the-thickness angle interlock - preform C of Table 1) following failure under uniaxial compression.

For woven composites, the response of the cuboidal specimens is entirely different (Fig. 3(b)). The maximum compressive load still occurs at similar compressive strain, but it is much lower in magnitude. There is substantially more nonlinearity in the stress-strain curve as the maximum load is approached. And, most striking of all, the material continues to bear more than 50% of the maximum load and substantially more than the neat resin out to compressive strains of 15% or more. Post-mortem examination reveals damage typified by Fig. 4(b): there is widespread debonding of warp weavers and stuffers from the surrounding matrix and stuffers have buckled and failed in many places. (Note that so-called debond cracks actually lie entirely within the matrix, rather than consisting even partly of interfacial microcracks between fibers and matrix.) There is no apparent correlation between the locations at which stuffers have failed in any specimen.

There is considerable variation in the strengths of the cuboidal specimens of the woven composites (Table 3). Some of this variation can be correlated with variations in the number of stuffers present in each specimen, as can be seen by comparison with the volume fractions of Table 3, which were estimated by counting stuffers and, for type A specimens, surface warp weavers in each specimen.

For the woven composites, the strain to maximum load, $\varepsilon_m$, is remarkably constant (± 3% variance), while there is a larger variation in strength (± 20%) and a much larger variation in modulus (± 40%). For the stitched laminates, in contrast, both $\varepsilon_m$ and strength vary by ± 20% and are correlated, while the modulus varies by only ± 8%.

Dog-bone Specimen Test Results

The dog-bone specimens were sufficiently large to allow the use of moiré interferometry to study the localized surface strains that accompany specimen failure. The moiré fringes of Fig. 5 show contours of constant displacement in the load direction for a type C specimen. Even though the strains are all elastic and reversible, since the load in Fig. 5 (80 MPa) is well below the composite yield strength, the influence of stuffers, fillers, and warp weavers is clearly visible. Significant local strain inhomogeneities result.

Figure 6 compares the axial strain from moiré fringes averaged over a 1 cm gauge length (to minimize the effect of inhomogeneity) with strains measured by clip gauges and by an alternative imaging technique. The alternative technique, described fully in (ref. 7), is based on comparing a digitized image taken under load to a reference image taken at zero load. The strains from all three methods are comparable.

Stress-strain histories measured for dog-bone specimens by clip-gauges are shown in Fig. 7 and numerical values of key features are summarized in Table 4. The strengths are smaller than those measured for cuboidal specimens, being comparable to the yield strength on the curves of Fig. 3. Figure 7 also shows a qualitative difference from Fig. 3, since, for all but type D specimens, there is a discontinuous drop in load after the maximum load. As for the cuboidal specimen tests, Table 4 shows remarkable constancy in strain to maximum load.

In all the tests of Table 4, post-mortem inspection of the specimens revealed that final failure was associated with a dominant shear band. This shear band was not as localized as the kink bands observed in cuboidal specimens of stitched laminates; and there was often extensive, ancillary damage visible elsewhere on the gauge section. However, the damage was far more localized than that in cuboidal specimens of woven composites, which always showed damage post mortem over the whole gauge section.

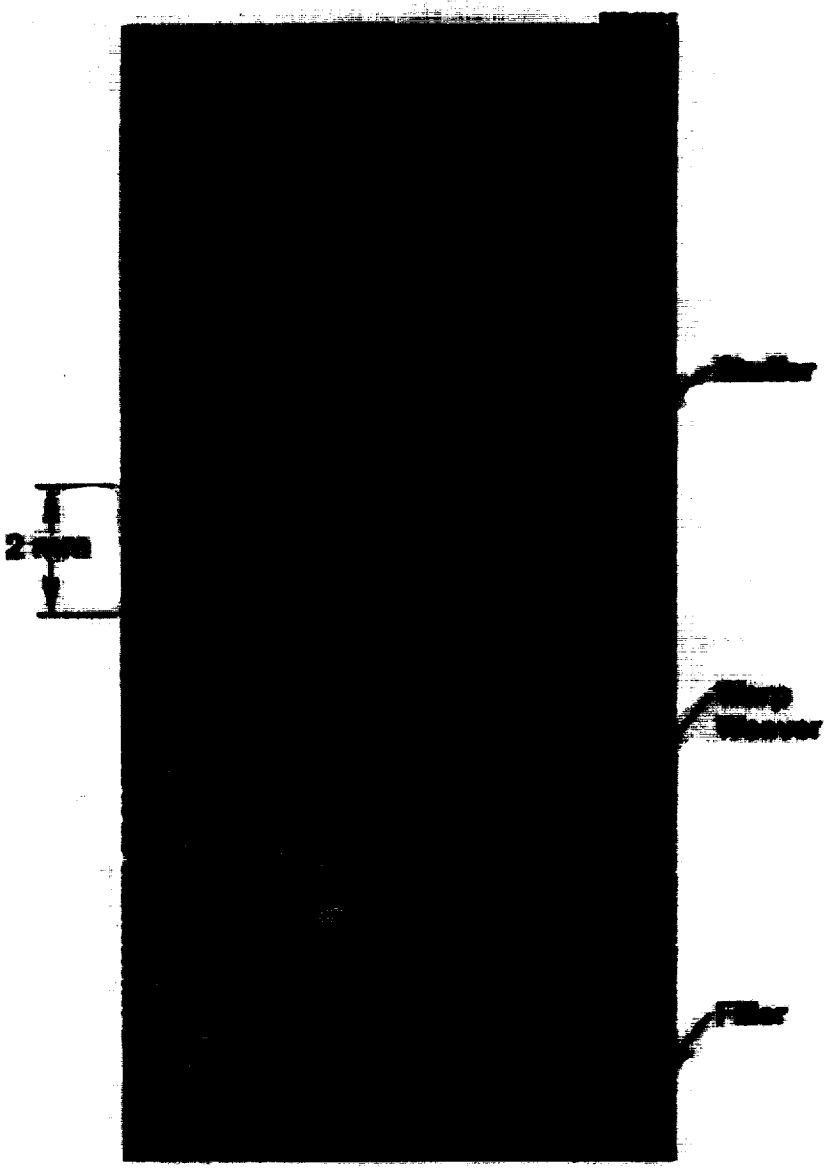

Fig. 5 Contours of constant displacement in the load direction measured by moiré interferometry. Stuffers, warp weavers, and some fillers have been outlined to emphasize their role in determining local strain variations.

### 3.2 Observations of Microscopic Cracking and Deformation

The digital imaging method was also used to assess local damage before and after the attainment of peak load (and the discontinuous load drop) in type A and C specimens. Observations prior to peak load were consistent with the moiré fringes of Fig. 5. Making measurements after the load drop is not straightforward, because there are many cracks and pieces of the composite move almost independently of one another. Nevertheless, it appears that the first initial deformation is associated with relatively long-ranged buckling of stuffers allowed by extensive systems of cracks aligned parallel to them. This produces a transverse swelling or barrelling of the composite. The buckling of neighboring stuffers shows some correlation, especially for type A specimens (layer-to-layer angle interlock). However, the development of a major shear band of the kind found to dominate the damage post-mortem did not occur until well beyond $\epsilon_m$: at 2% strain for type C specimens and 4% strain for type A. Thus the discontinuous load drop is evidently associated not with a kink band but with the buckling failure of individual stuffers.

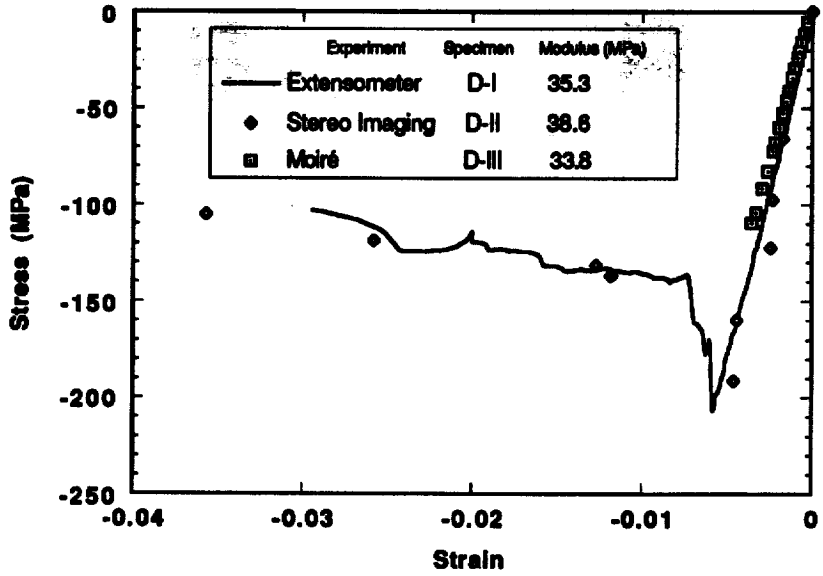


Fig. 6 Strain-load histories for dog-bone specimens of type D woven composites under uniaxial compression measured by several methods.

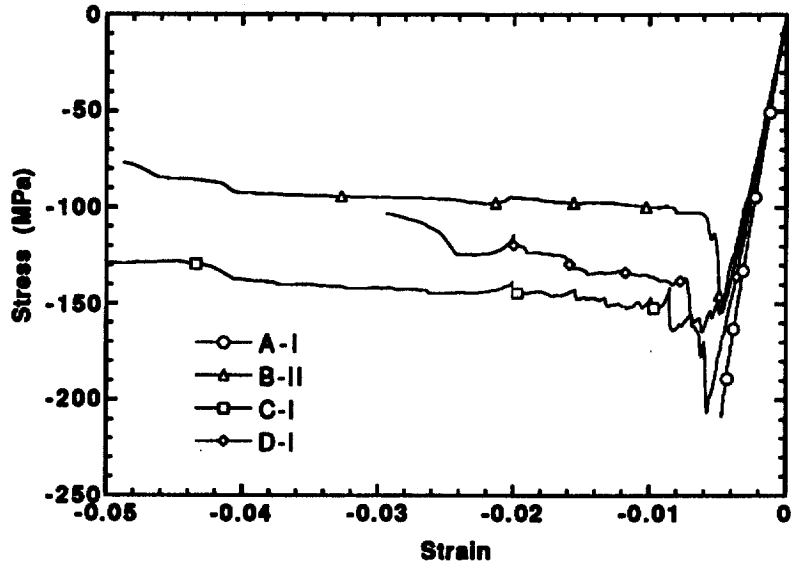


Fig. 7 Stress vs strain for dog-bone specimens.

## 4. CONCEPTS IN STRENGTH AND DAMAGE TOLERANCE

Comparison of cuboidal specimens of stitched laminates and woven composites under monotonic compression has shown that the former have about twice the strength while the latter have the greater strain to failure by an order of magnitude. Further tests on dog-bone specimens show that in fact woven composites may also exhibit discontinuous load drops, as observed for the stitched laminates, when there is less constraint imposed by the loading grips. But they always retain large strains to total failure. In this section, some mechanistic arguments will be presented to try to account for these observations at least qualitatively. The arguments lead to the interesting prospect of achieving an optimal compromise between strength and damage tolerance by appropriate choice of reinforcement architecture.

### 4.1 The Role of Fiber Volume Fraction

Consider first the observed relationship between strength and the volume fraction, $v_s$, of fibers aligned along the stress axis (Tables 1 and 2). Generally speaking, both the modulus and the compressive strength would be expected to increase as $v_s$ increases. Yet $v_s \approx 0.16$ for the stitched laminates (Table 1), which is less than the values for the woven composites (Table 2), while the stitched laminates are far stiffer and stronger. Much of this difference may be attributable to the degree of straightness of the primary load bearing fibers: the coarser fiber architecture of the woven composites probably leads to greater initial curvature of the stuffers than exists in the 0° fibers in the stitched laminates. Further research in which stuffer alignment is controlled more carefully during impregnation and cure is required to quantify this effect.

While fiber volume fraction does not account for the differences between stitched laminates and woven composites, variations of strength within the latter class are correlated with fiber volume fraction, as evidenced by Tables 3 and 4.

### 4.2 Damage Propagation - The Stability of Kink Bands

The events that follow the buckling and failure of the first stuffer in a woven composite or the first bundle of 0° fibers in a stitched laminate depend on whether neighboring aligned fibers are loaded beyond their failure limit and the degree to which shear displacements are constrained. If the first buckling and failure have occurred at an unusually low stress, neighboring aligned fibers will be less likely to be critically loaded even under the effects of load redistribution; and if shear displacements are constrained, that too will help preserve neighboring fibers by minimizing the stress concentration around the first failure.

In stitched laminates, the first buckling and failure always led in the tests reported here to immediate failure by an unstable kink band. In these materials, the first buckling and failure do not occur at an unusually low stress; the 0° tows are relatively straight and closely packed amongst other plies and the stitching tows are orthogonal to the load axis and do not appear to lower the load at which buckling and failure of 0° fibers occur. Thus the compressive strength is relatively high and, when one bundle of 0° fibers eventually does buckle, the concomitant stress concentration acting on neighboring fibers is sufficient to cause their immediate buckling too, because the applied load is already close to their failure load. Thus a kink band forms and propagates unstably across the whole specimen even for tests of cuboidal specimens, where constraint of the shear displacement required for the kink band to propagate is greatest; the stress-strain history is characteristic of a brittle material. Kink band failure is very common in aligned continuous fibers under compression (see, for example, ref. 8).

In the angle interlock specimens, on the other hand, the relative coarseness of the structure, the presence of thick warp weavers, and the initial curvature of the stuffers all facilitate early buckling failures. The moiré fringes of Fig. 5 clearly show segments of stuffers buckling out of the specimen even in the elastic regime. Such inhomogeneity also implies that, when the first buckling failures of stuffers occur, they will do so at sites uncorrelated with other weak areas - cp. the distribution of early buckling sites in Fig. 5. Furthermore, since the first buckling failures occur at relatively low stresses and stuffers are relatively well separated in the woven structures, adjacent stuffers are not generally loaded above their failure stress in the stress concentration around a failure site. Thus the formation of the eventually fatal shear band is deferred to higher strains.

As for the load, it falls following the first stuffer failures simply because the specimen compliance rises when the volume fraction of intact stuffers is reduced. The stress-strain history is that of a ductile material.

### 4.3 Possible Design Paths for Future Woven Composites

The overall picture is thus one of compromising strength and strain to failure (or damage tolerance). The open, coarser structure of the woven composites may be considered as containing intrinsic flaws, consisting of fluctuations in geometry that lead to local failure sites. The flaws lead to lower strength, but they tend to cause damage to be spatially distributed, in which case failure is not by the catastrophic mechanism of an unstably propagating kink band, but by the attainment of a critical density of broadly distributed damage.

Since the potency of the flaws is proportional to their size, it can be predicted that, as the scale of the woven architecture becomes finer and finer, e.g. by reducing the denier of all tows, the strength should rise to the limit of that of the stitched laminates while the material should become increasingly brittle. The reduction in the scale of the reinforcement may be thought of as producing a more homogeneous composite populated by flaws of decreasing size.

## CONCLUSIONS

Strength and strain to failure under uniaxial compression are strongly influenced by the geometry of the fiber reinforcement in 3D composites and the degree to which lateral displacements are constrained in tests. An open, coarse structure lowers strength but promotes high strain to failure or damage tolerance. In the angle interlock weaves studied, reinforcement inhomogeneity led to early buckling and failure of stuffers. This favored a wide spatial distribution of damage, in contrast to the localized kink bands that always cause failure in stitched laminates. If damage is delocalized, high strain to failure is assured.

## ACKNOWLEDGMENTS

Work funded by NASA Langley Research Center under contract number NAS1-18840. The authors are deeply indebted to Dr. David Marshall for many fruitful conversations.

## REFERENCES


1. M.B. Dow and D.L. Smith, "Damage Tolerant Composite Materials Produced by Stitching Carbon Fabrics," Int. SAMPE Tech. Conf. Series 21, 595-605 (1989).

2. R.E. Horton and J.E. McCarty, "Damage Tolerance of Composites," in Engineered Materials Handbook, Vol. 1, "Composites," ed. C.A. Dostal, ASM Int., Metals Park, Ohio, 1987.

3. P.J. Smith and R.D. Wilson, "Damage Tolerant Composite Wing Panels for Transport Aircraft," Boeing Commercial Airplane Company, NASA Contractor Report 3951.

4. R. Palmer, M.B. Dow, and D.L. Smith, "Development of Stitching Reinforcement for Transport Wing Panels," in Proc. First NASA Advanced Composites Technology Conference, NASA Conf. Publ. 3104, pp. 621-46.

5. R. Palmer and F. Curzio, "Cost Effective Composites Using Multi-Needle Stitching and RTM/VIM," in Fiber-Tex 1988 Conference, Greenville, South Carolina, September 13-15, 1988. NASA CP-3038, June 1989.

6. M. Piggott, "Load Bearing Fiber Composites," Pergamon, Oxford, 1980.

7. M.R. James, W.L. Morris, and B.N. Cox, "A High Accuracy Automated Strain Field Mapper," Exptl. Mech. 30, 60-67 (1990).

8. N. Fleck and B. Budiansky," Compressive Failure of Fiber Composites," J. Mech. Phys. Solids, in press.

**Table 1**

**Characteristics of the Stitched Laminates**

| Material Label | Stitching Tows | Density ($g/cm^3$) | 0° stitches per cm (inch) | 90° stitches per cm (inch) | Volume fraction of stitches | $\nu_s$ (a) |
|---|---|---|---|---|---|---|
| SL-Kevlar | 1.5k denier Kevlar-29 | 1.45 | 12.7 (5.0) | 9.2 (6.0) | 0.016 | 0.16 |
| SL-Fiberglass | 3.57k denier S-2 glass | 2.48 | 23 (9.0) | 23 (9.0) | 0.036 | 0.16 |
| SL-Graphite | 1.44k denier Toray-900 graphite | 1.8 | 20 (8.0) | 23 (9.0) | 0.019 | 0.16 |

(a) Volume fraction of 0° AS4 fibers.

**Table 2**

**Architectures, Materials, and Fiber Densities in TTI Angle Interlock Preforms**

| Preform Label | Architecture | Warp Weaver Material | Ends per cm (inch)(a) | Picks per cm (inch)(b) | Specimen Thickness (cm)(c) | $\nu_s$ (d) | $\nu_f$ (e) | $\nu_w$ (f) |
|---|---|---|---|---|---|---|---|---|
| A | layer-to layer | AS4 | 5.1 (13) | 4.4 (11.3) | 1.26 | 0.210 | 0.229 | 0.064 |
| B | layer-to layer | S-2 glass | 5.1 (13) | 5.9 (15) | 1.24 | 0.214 | 0.308 | 0.031 |
| C | through-the thickness | AS4 | 4.7 (12) | 5.0 (12.7) | 1.02 | 0.240 | 0.317 | 0.073 |
| D | through-the thickness | S-2 glass | 5.1 (13) | 5.0 (12.7) | 0.97 | 0.273 | 0.334 | 0.040 |

(a) i.e., number of columns of stuffers per inch in weft direction.
(b) i.e., number of columns of fillers per inch in warp direction.
(c) in direction normal to warp and weft directions.
(d) $\nu_s \equiv$ volume fraction of stuffer (straight warp) tows.
(e) $\nu_s \equiv$ volume fraction of filler (weft) tows.
(f) $\nu_w \equiv$ volume fraction of body warp weaver (3D warp) tows.

Table 3

Data for Cuboidal Test Specimens

| | Specimen Label | Modulus (GPa) | Maximum Compressive Stress (Msa) | $v_s$[b] | $\varepsilon_m$[c] | $\varepsilon_{1/2}$[d] |
|---|---|---|---|---|---|---|
| Woven Composites[a] | A-1 | 14 | 230 | 0.28 | 0.019 | 0.07 |
| | B-1 | 11.5 | 215 | 0.23 | 0.020 | 0.10 |
| | B-2 | 11 | 205 | 0.20 | 0.020 | 0.12 |
| | C-1 | 17 | 240 | 0.33 | 0.020 | 0.16 |
| | C-2 | 15 | 205 | 0.27 | 0.020 | 0.15 |
| | C-3 | 16 | 200 | 0.25 | 0.019 | 0.16 |
| | D-1 | 14.5 | 240 | 0.27 | 0.019 | 0.1 |
| Tactix 138 epoxy | e-1 | 2.55 | 105 | | 0.079 | -[e] |
| | e-2 | 2.75 | 115 | | 0.080 | -[e] |
| Stitched Laminates | SL-Kevlar-1 | 18 | 360 | | 0.025 | -[f] |
| | SL-Kevlar-2 | 19.5 | 380 | | 0.022 | -[f] |
| | SL-Fiberglass-1 | 17 | 425 | | 0.028 | -[f] |
| | SL-Fiberglass-2 | 18.5 | 430 | | 0.026 | -[f] |
| | SL-Graphite-1 | 19.5 | 495 | | 0.03 | -[f] |

(a) The letter in labels for woven composites refers to preform label of Table 2.
(b) Including straight surface warp weavers.
(c) Compressive strain at maximum load.
(d) Compressive strain when post-peak load has fallen to half the maximum.
(e) Test finished with load still exceeding half maximum.
(f) Essentially identical to $\varepsilon_m$.

Table 4

Data for Dog-Bone Test Specimens

| Specimen Label | Controlled Parameter | Maximum Compressive Stress (MPa) | Modulus (GPa) | $\varepsilon_m$[b] 0.5" | $\varepsilon_m$[b] 0.12" | $\varepsilon_{1/2}$[c] 0.5" |
|---|---|---|---|---|---|---|
| A-I[a] | strain | 210 | 41.37 | $5 \times 10^{-3}$ | | |
| A-II | load | 210 | 28 | | $1.7 \times 10^{-2}$ | |
| B-I | load | 140 | 25 | $6 \times 10^{-3}$ | | |
| B-II | strain | 155 | 34.75 | $5 \times 10^{-3}$ | | $5 \times 10^{-2}$ |
| B-III | strain | 160 | | | | |
| C-I | strain | 165 | 32.4 | $5.1 \times 10^{-3}$ | | $1.4 \times 10^{-1}$ |
| C-II | load | 150 | | | $8.5 \times 10^{-3}$ | |
| D-I | strain | 205 | 35.5 | $6 \times 10^{-3}$ | | $3 \times 10^{-2}$ |
| D-II | strain | 195 | 38.6 | $5 \times 10^{-3}$ | | $4 \times 10^{-2}$ |

(a) The letter in the labels refers to the preform labels of Table 2.
(b) Compressive strain at maximum load.
(c) Compressive strain when post-peak load has fallen to half of maximum.